Practical Guide to Quantum Phase Transitions in Quantum-Dot-Based Tunable Josephson Junctions

A. Kadlecová,[1] M. Žonda,[1,2] V. Pokorný,[1] and T. Novotný[1,*]

[1] *Department of Condensed Matter Physics, Faculty of Mathematics and Physics, Charles University in Prague, Ke Karlovu 5, Praha 2 CZ-121 16, Czech Republic*

[2] *Institute of Physics, Albert Ludwig University of Freiburg, Hermann-Herder-Strasse 3, Freiburg 791 04, Germany*

(Received 18 July 2018; revised manuscript received 1 April 2019; published 30 April 2019)

Quantum dots attached to BCS superconducting leads exhibit a $0-\pi$ impurity quantum phase transition, which can be experimentally controlled either by the gate voltage or by the superconducting phase difference. For the pertinent superconducting single-impurity Anderson model, we present two simple analytical formulae describing the position of the phase boundary in parameter space for the weakly correlated and Kondo regime, respectively. Furthermore, we show that the two-level approximation provides an excellent description of the low-temperature physics of superconducting quantum dots near the phase transition. We discuss reliability and mutual agreement of available finite-temperature numerical methods (numerical renormalization group and quantum Monte Carlo) and suggest an alternative approach for efficient determination of the quantum phase boundary from measured finite-temperature data. Our results enable fast and efficient, yet reliable characterization and design of such nanoscopic tunable Josephson-junction devices.

DOI: 10.1103/PhysRevApplied.11.044094

I. INTRODUCTION

Low-temperature nanostructures involving quantum dots attached to superconductors have been intensively studied in the past two decades—see Ref. [1] for theoretical and Ref. [2] for experimental overviews. A number of various setups involving several superconducting and/or normal leads have been thus far realized using a variety of systems (single molecules such as C_{60}, carbon nanotubes, semiconducting InAs nanowires etc.) as the central functional element (quantum dot) [3–28]. Parameters of such systems are typically tunable by gate voltage, which changes the single-particle energies on the dot, and in the case of superconducting quantum interference device (SQUID) setups by the magnetic flux through the loop tuning the phase difference across these generalized Josephson junctions. Their envisioned applications range from various sensors and detectors (e.g., single-molecule SQUIDs [9,29]) to building blocks of quantum-information technologies [2].

One of the simplest setups involves a quantum dot attached to just two superconducting leads whose relative superconducting phase difference φ can be tuned leading to the flow of the Josephson supercurrent through the junction. Very often such a system can be even quantitatively described by the single-impurity Anderson model (SIAM) coupled to BCS leads [30], which exhibits an impurity quantum phase transition. This so-called $0-\pi$ transition corresponds to the change of the system ground state from a nonmagnetic singlet to a spin-degenerate doublet and is accompanied by the sign change of the supercurrent (from positive in the 0 phase to negative in the π phase) [7,9,10,16,20,24–27] and crossing of the Andreev bound states (ABSs) at the Fermi energy [18,22,26,31]. Depending on the relative strength of the on-dot Coulomb interaction the 0-phase ground-state singlet can be predominantly BCS-like (for weak interaction) or Kondo-like (strong correlations) with a broad cross-over between these two limiting cases. This physical picture has been firmly established over the years by various analytic and numeric theoretical methods [30,32–42] and fully qualitatively confirmed already by pilot experiments [7,9,10].

However, recent experiments using the SQUID setup allowing a high level of tunability [24–27] have revealed difficulties involved in making a quantitative comparison with theory. Heavy numerical tools such as quantum Monte Carlo (QMC) or numerical renormalization group (NRG) turn out to be too costly as for the computational resources to allow for broader scans throughout the model parameter space, which are necessary for an efficient and reliable identification of the experimental situation. They seem to be quite inconvenient for the initial phase of

*tno@karlov.mff.cuni.cz

the data analysis, which should place the given experimental setup into the proper context of rough parameter values, and for capturing the global trends induced by coarse-grained parameter changes.

This task rather calls for a simple, ideally analytical, or very efficient numerical technique, which would parse the parameter space grossly. As a next step, more elaborate methods including QMC and/or NRG could be used to fine tune the parameters, yet taking into account the common experimental accuracy of 10%–20%, quite often these precise methods may not be required at all. Here, we offer two simple analytical formulae for the position of the $0-\pi$ phase boundary in the complementary weakly interacting and strongly correlated (Kondo) regimes, respectively. They are based on the combination of analytical insights and NRG data and with a reasonable precision cover a big part of the SIAM parameter space.

Another issue concerns finite temperatures: the phase boundary is a ground-state, i.e. zero-temperature quantity but the experiments are naturally performed at finite (even if ideally very small) temperatures. The task of extrapolating to zero temperature from finite-temperature experimental data is principally nontrivial and, as we show, it has not been so far addressed properly. We identify a very simple and straightforward method how to extract zero-temperature quantities directly from finite-temperature data without the need for any postprocessing.

II. MODEL AND NOTATION

As explained above, we consider the single-impurity Anderson model of a quantum dot connected to two BCS superconducting leads. The full Hamiltonian reads

$$\mathcal{H} = \mathcal{H}_{\rm dot} + \sum_{\alpha} (\mathcal{H}^{\alpha}_{\rm lead} + \mathcal{H}^{\alpha}_{T}), \tag{1a}$$

where $\alpha = L, R$ denotes the left and right superconducting leads. The dot Hamiltonian

$$\mathcal{H}_{\rm dot} = \varepsilon \sum_{\sigma=\uparrow,\downarrow} d^{\dagger}_{\sigma} d_{\sigma} + U d^{\dagger}_{\uparrow} d_{\uparrow} d^{\dagger}_{\downarrow} d_{\downarrow} \tag{1b}$$

describes an impurity with the spin-degenerate single-particle level ε and the local Coulomb interaction U in the case of the doubly occupied dot. Operators $d^{\dagger}_{\sigma}$ (d_{σ}) create (annihilate) on-dot electrons with spin σ. The BCS Hamiltonian of the superconducting leads is

$$\mathcal{H}^{\alpha}_{\rm lead} = \sum_{\mathbf{k}\sigma} \varepsilon_{\alpha}(\mathbf{k})\, c^{\dagger}_{\alpha\mathbf{k}\sigma} c_{\alpha\mathbf{k}\sigma} - \Delta_{\alpha} \sum_{\mathbf{k}} (e^{i\varphi_{\alpha}} c^{\dagger}_{\alpha\mathbf{k}\uparrow} c^{\dagger}_{\alpha-\mathbf{k}\downarrow} + \text{H.c.}), \tag{1c}$$

where $c^{\dagger}_{\alpha\mathbf{k}\sigma}$, $c_{\alpha\mathbf{k}\sigma}$ are the creation and annihilation operators of electrons with momentum $\mathbf{k}$ and spin σ, Δ_{α} is the amplitude of the superconducting gap in the lead α, and φ_{α} is its superconducting phase. We denote by $\varphi \equiv \varphi_L - \varphi_R$ the phase difference between the two superconducting leads. The last term in Eq. (1a) is the tunnel-coupling Hamiltonian

$$\mathcal{H}^{\alpha}_{T} = \sum_{\mathbf{k}\sigma} (t_{\alpha\mathbf{k}} c^{\dagger}_{\alpha\mathbf{k}\sigma} d_{\sigma} + \text{H.c.}), \tag{1d}$$

with $t_{\alpha\mathbf{k}}$ denoting the tunneling matrix elements. We assume the tunnel-coupling magnitudes $\Gamma_{\alpha}(\varepsilon) \equiv \pi \sum_{\mathbf{k}} |t_{\alpha\mathbf{k}}|^2 \delta[\varepsilon - \varepsilon_{\alpha}(\mathbf{k})]$ to be constant in the energy range of interest $\Gamma_{\alpha}(\varepsilon) \simeq \Gamma_{a}$.

The model is described by just a few parameters: the dot-level energy ε (which can be experimentally tuned by the gate voltage), the local Coulomb interaction between dot electrons U, the total coupling strength $\Gamma \equiv \Gamma_L + \Gamma_R$ and the tunnel asymmetry of the setup $a = \Gamma_L/\Gamma_R$, the phase difference φ (which, if the junction is a part of a SQUID, can be controlled by an applied magnetic field [7,9,20,24–27]), and the superconducting gaps Δ_{α}. Throughout this whole article we assume the generic experimental situation of equal gaps $\Delta_L = \Delta_R \equiv \Delta$, which implies that we can use the symmetry-asymmetry relation discovered in Ref. [43] to simplify the model by introduction of the compact quantity

$$\chi = \chi(\varphi, a) \equiv 1 - \frac{4a}{(a+1)^2} \sin^2 \frac{\varphi}{2}, \tag{2}$$

on which the on-dot quantities (including especially the phase boundary) exclusively depend, i.e., the two parameters a and φ are reduced to a single one χ.

For the normal-state Kondo temperature we use the expression based on Wilson's definition via magnetic susceptibility [44,45]

$$k_B T_K \equiv 0.29\sqrt{\Gamma U} \exp\left(-\frac{\pi|\varepsilon|(\varepsilon+U)}{2\Gamma U}\right). \tag{3}$$

Eventually, we further use (when convenient) the shifted and normalized level energy

$$\tilde{\varepsilon} \equiv \frac{\varepsilon + U/2}{U/2} = 1 + \frac{2\varepsilon}{U}, \tag{4}$$

a dimensionless number, which is zero at half filling ($\varepsilon = -U/2$).

III. ZERO-TEMPERATURE PHASE BOUNDARIES

For ground states, features of the system are known to be well captured by the NRG. However, these computations can be time consuming and it is therefore advantageous to have other, possibly less precise but significantly easier tools at hand. In two complementary limits we have found

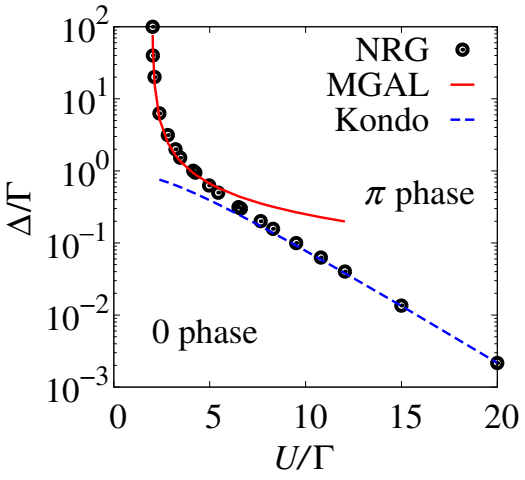

FIG. 1. Phase diagram for the superconducting SIAM at half filling ($\varepsilon = -U/2$) and $\chi = 1$ ($\varphi = 0$). We illustrate the ranges of validity of the formulae given in Secs. III A and III B. Black bullets represent numerical renormalization group data, the red line is the MGAL prediction (5), and the blue dashed line corresponds to $\Delta_C \approx 4.29 T_K$ given by Eq. (7) for $\chi = 1$.

simple analytical formulae which capture the position of the $0-\pi$ phase boundary in the parameter space. The "MGAL" approximation presented in Sec. III A deals with the weakly correlated regime characterized by moderate U/Γ ratios. On the other hand, in Sec. III B we comment on the strongly correlated Kondo regime of the quantum dot, taking into account the χ (φ) dependence. Figure 1 illustrates the ranges of validity of our predictions. At half filling ($\tilde{\varepsilon} = 0$) and for $\chi = 1$ ($\varphi = 0$) the MGAL approximation is valid up to $U/\Gamma \lesssim 5$. On the other hand, Kondo physics prevails for $U/\Gamma \gtrsim 7$. The intermediate range can be well and very fast captured by the numerical solution of the second-order perturbation theory of Refs. [46] and [47] (in particular, see Fig. 6 in Ref. [47]) for which we provide publicly accessible code [48].

A. Weakly correlated regime

By analyzing NRG data obtained by the "NRG Ljubljana" code [49] we find (for more details see the Appendix) that for the weakly correlated quantum-dot regime, the phase boundary can be approximated with the equation

$$\chi = \mathcal{U}^2 - \mathcal{U}(\mathcal{U}+1)\tilde{\varepsilon}^2, \tag{5}$$

where

$$\mathcal{U} \equiv \frac{U}{2\Gamma}\frac{\Delta}{\Gamma+\Delta} \tag{6}$$

and $\chi = \chi(\varphi, a)$, $\tilde{\varepsilon}$ are given by Eqs. (2) and (4), respectively. For $\chi = 1$ ($\varphi = 0$) the relation (5) reduces to $1 - \tilde{\varepsilon}^2 = 1/\mathcal{U}$. We call Eq. (5) the modified generalized atomic limit (MGAL), referring to the previously derived generalized atomic limit (GAL) approximation [46,47], which is identical to MGAL at the half filling $\tilde{\varepsilon} = 0$.

To illustrate the agreement of Eq. (5) with the NRG data, we present zero-temperature phase diagrams for different parameter subspaces in Fig. 2, namely the $\Gamma - \varepsilon$ phase diagram in Fig. 2(a), the $\Gamma - U$ diagram away from half filling in Fig. 2(b) and, finally, several phase-transition boundaries in the $\chi - \tilde{\varepsilon}$ ($\varphi - \varepsilon$) plane in Fig. 2(c). Equation (5) is mostly in a pretty good agreement with the NRG and significantly outperforms previously known analytic formulas, including the atomic limit [40,50], Hartree-Fock prediction, and the GAL away from half filling [46,47]. We therefore suggest it as a simple first estimate of the position of the phase boundary in the weakly correlated regime (cf. Fig. 1).

A more elaborate method of determining the phase boundary in the weakly correlated regime is the second-order perturbation theory [46,47]. This method is based on the perturbation expansion technique in the Coulomb interaction U. Although this method is unable to describe the π phase due to its double-degenerate ground state, it provides reliable description of the 0 phase, including its phase boundary up to $U/\Gamma \approx 10$ (not too far from half filling), see Fig. 2(c). This method is numerical and, consequently, it is much harder to implement than analytical MGAL, nevertheless an efficient, free, and easy-to-use Python code called SQUAD is available [48]. Numerical perturbative calculations are orders of magnitude faster than the NRG code and constitute a very reasonable compromise between the accuracy and numerical costs in the weak-to-moderately correlated regime. For all possible aspects and details of the perturbation theory we refer the reader to Ref. [47].

B. Kondo regime

In the Kondo regime the phase boundary is widely believed to be a universal function of T_K/Δ and specifically to occur at $T_K \approx \Delta$. In Ref. [43] we argued that the coupling asymmetry a must play some role, however, we left the question of universality open. This section establishes that the phase boundary can indeed be described by a universal function of T_K/Δ if $\chi = \chi(\varphi, a)$ given by Eq. (2) is used as a variable.

The formula for the critical value of the gap Δ_C determined from the NRG data [Fig. 3(a)] and valid for our definition of T_K (3) (if another convention is used, the formula should be properly rescaled) reads

$$\frac{\Delta_C}{k_B T_K} = \exp\left(\alpha\sqrt{\chi}\right) - 1, \tag{7}$$

where $\alpha \approx 5/3$. More accurately, we fit three different sets of numerical data [shown in Fig. 3(a)] and we find that $\alpha_1 = 1.65 \pm 0.02$ for $U/\Gamma = 20$, $U = 0.1D$, $\alpha_2 = 1.67 \pm$

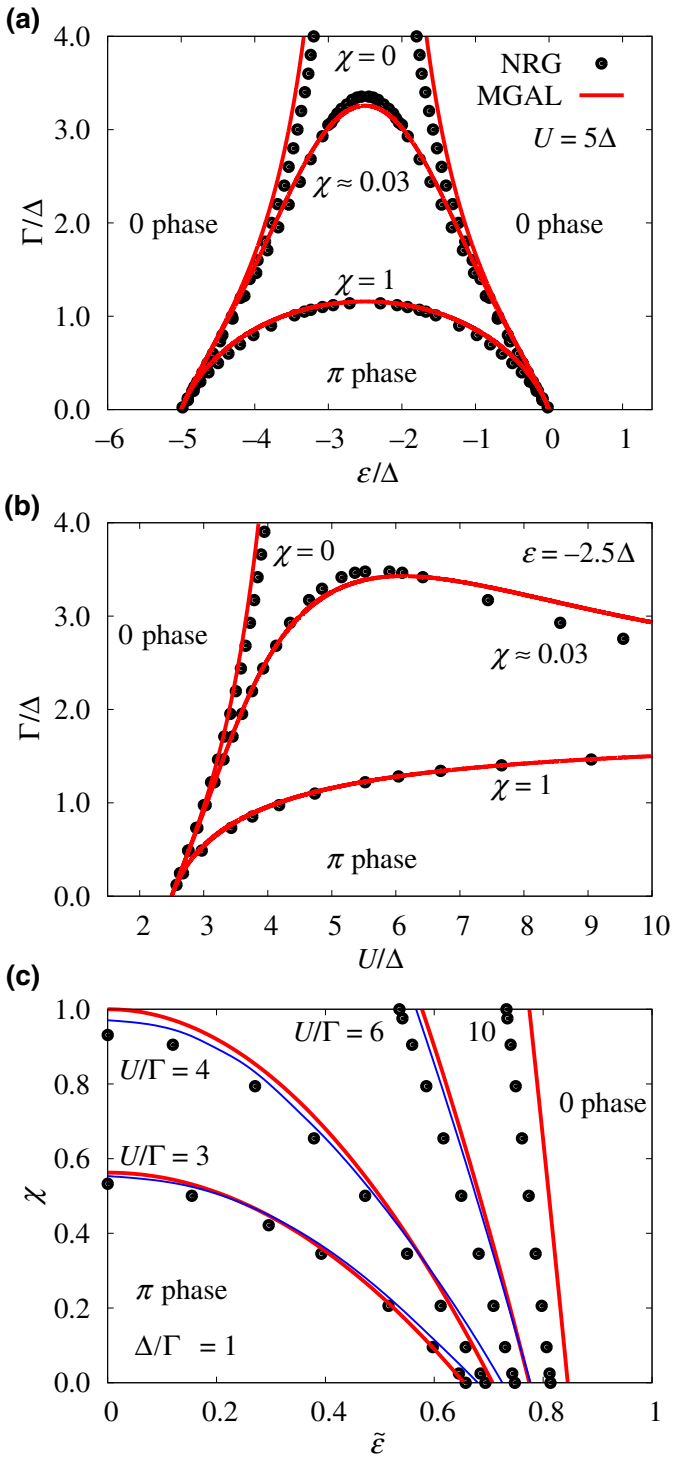

FIG. 2. Zero-temperature phase diagrams of the superconducting quantum dot in the weakly correlated regime. Black bullets represent NRG data, while the red line is the prediction by the MGAL formula (5) and blue lines in (c) are the second-order perturbation-theory solutions. (a) $\Gamma - \varepsilon$ dependence for a junction with $U = 5\Delta$. The phase boundary is shown for $\chi = 1$, $\chi = 0$ and a small but nonzero $\chi = 0.0325$. (b) $\Gamma - U$ dependence away from half filling ($\varepsilon = -2.5\Delta$). (c) $\chi - \tilde{\varepsilon}$ dependence for different U/Γ ratios ($U/\Gamma = 3$, 4, 6, and 10) at $\Gamma = \Delta$.

0.02 for $U/\Gamma = 15$, $U = 0.15D$, and $\alpha_3 = 1.69 \pm 0.03$ for $U/\Gamma = 15$, $U = 0.015D$, where D is the bandwidth used in the NRG calculations. Ideally the calculation should be performed in the limit of an infinite band, hence the (necessary) choice of a finite D influences the numerical results slightly.

The dependence in Fig. 3(a) is calculated at half filling, $\tilde{\varepsilon} = 0$. Figure 3(b) reveals that $\tilde{\varepsilon}$ dependence is very weak up to $\tilde{\varepsilon} \approx 0.4$, significantly departing from the value predicted by Eq. (7) for $\tilde{\varepsilon} \approx 0.6$. For $\chi = 0$, which can only be achieved for $\varphi = \pi$ in a perfectly symmetric junction with $a = 1$ [43], and exactly at half filling, there is no phase transition, but a small critical gap is found with any departure from half filling [51]. Results in Fig. 3(b) are in agreement with Ref. [[35], Fig. 9a]. Authors of this previous study have tested the ε independence for two different values of U/Γ and concluded that the universality breaks down in the valence fluctuation regime $|\varepsilon| \lesssim \pi\Gamma$ ($|\tilde{\varepsilon}| \gtrsim 1 - 2\pi\Gamma/U \approx 0.58$).

As given by Eq. (7), for $\chi = 1$ (corresponding to $\varphi = 0$) the phase transition appears (for our definition of T_K and $\alpha = 5/3$) at $\Delta_C/T_K \approx 4.29$. For any nonzero φ the critical gap will be smaller.

IV. FINITE TEMPERATURES

In superconducting quantum-dot devices the $0 - \pi$ transition reflects an underlying impurity quantum phase transition between the singlet and doublet ground states, a crossing of the two lowest-energy many-body levels. At zero temperature, the quantum critical point (QCP) is clearly signaled by a jump in the supercurrent and the change of its sign, however with increasing finite temperature the current-phase relation (CPR) becomes continuous and the point where the supercurrent changes sign shifts away from the QCP. This complicates the determination of the position of the QCP from real experimental data, as well as from the results of strictly finite-temperature numerical methods such as QMC. In Sec. IV A, we present a simple physical argument that the crossing point of the finite temperature current-phase relations coincides with the QCP at low enough temperatures. Moreover, the crossing can be observed not only for the current as a function of the phase difference but basically for any physical quantity as a function of any parameter that induces the singlet-doublet phase transition. We further discuss the temperature range of applicability of the underlying two-level approximation and why previously used methods of estimating the QCP from the zero crossing of the Josephson current lead to inaccurate results (Sec. IV B). The two-level approximation expressed in Eq. (8) does not only hold for our system but is universally applicable to impurity quantum phase transitions of the first order regardless of their physical realization and microscopic origin.

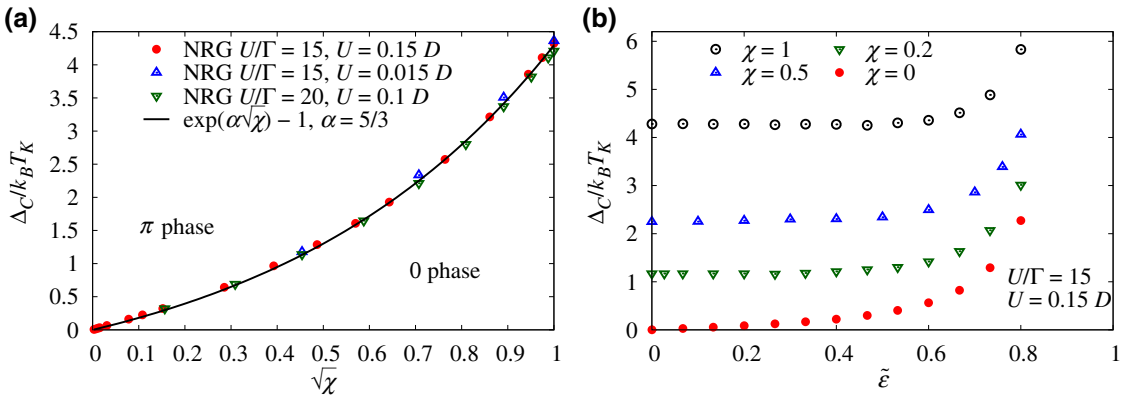

FIG. 3. (a) Universal shape in the Kondo regime of the ratio of the critical value of the gap Δ_C over the Kondo temperature T_K Eq. (3) as a function of variable χ Eq. (2). Points represent NRG data with $U/\Gamma = 15,\ 20$ and different values of the bandwidth D. The solid line corresponds to $\Delta_C/k_BT_K = \exp(\alpha\sqrt{\chi}) - 1$ with $\alpha = 5/3$. (b) The $\tilde{\varepsilon}$ dependence of Δ_C/T_K for $\chi = 0,\ 0.2,\ 0.5,$ and 1.

Finite-temperature results can be obtained by two complementary numerically exact methods, namely the NRG and QMC. NRG is a reliable method for the ground-state properties. It can also provide trustworthy results for low enough temperatures but the high ones are usually beyond its scope. On the other hand, the QMC is ideal for high temperatures but its computational demands rapidly increase with decreasing temperature. For quantum dots, there is a temperature range where both NRG and QMC are commonly used, but accuracy of both finite-temperature NRG and low-temperature QMC is sometimes subject to questions. Also, while for single quantum dots such as our system NRG is generally less computationally demanding than QMC, for more complicated setups such as multiple quantum dots or dots connected to multiple terminals QMC quickly becomes the method of choice. It is therefore highly desirable to establish whether these two methods are in agreement for systems where their ranges of applicability overlap. Therefore, we test the compatibility of both methods for our finite-temperature data.

In our calculations we use finite-temperature NRG from the "NRG Ljubljana" code [49], while QMC is done using the TRIQS/CTHYB continuous-time hybridization-expansion solver [52]. The superconducting pairing is introduced to the QMC method using a canonical particle-hole transformation in the spin-down sector, mapping the system to an impurity Anderson model with attractive interaction [53,54]. The comparisons of the two methods are shown in Figs. 4(a) and 6, where in the overlapping temperature range the NRG and QMC data coincide within the QMC error bars. The agreement implies that both methods are reliable for the experimentally relevant range of temperatures.

A. Low-temperature physics: two-level approximation

For low temperatures, the lowest (many-body) energy levels of a system become most significant. Due to the superconducting gap of single-particle excitations in our system, the lowest-lying states are discrete. In the spin-degenerate case (without external magnetic field) considered here there may be one or two discrete excited states below the single-particle continuum starting at the gap. We are mainly interested in the vicinity of the QCP where just one of these discrete excited states exchanges its role with the ground state (one of these two is a singlet and the other doublet). The other excited state, if it exists as a discrete state, is much higher in energy and can be neglected together with the continuum. We now formalize and show some consequences of this idea.

Starting with the canonical average $\bar{X} \equiv (1/Z)\sum_i X_i \exp(-\beta E_i)$ of an observable X, we explore the low-temperature regime $k_BT \ll \Delta$. As discussed above we can approximate the sum by taking the two lowest-energy states only. We obtain

$$X(y,\ T) \simeq \frac{X_S(y)e^{-\beta E_S(y)} + 2X_D(y)e^{-\beta E_D(y)}}{e^{-\beta E_S(y)} + 2e^{-\beta E_D(y)}}, \qquad (8)$$

where $X_{S(D)}$ is the zero-temperature value of the observable in the singlet (doublet) state, $E_{S(D)}$ is the associated energy of the singlet (doublet; factor 2 reflects its twofold degeneracy) state, y is any model parameter (e.g., the phase difference φ), and $\beta \equiv 1/k_BT$. Note that the fraction can be reduced by $e^{-\beta E_S(y)}$ to let it depend only on the energy difference corresponding to the energy of the Andreev bound states, $E_{\mathrm{ABS}}(y) \equiv E_D(y) - E_S(y)$.

To illustrate the physics of Eq. (8), in Fig. 4(a) we present the dependence of the supercurrent on temperature for three chosen values of ε from the vicinity of the phase transition. The empty circles with points are calculated with the NRG, while full circles with error bars represent the QMC results (for more specification and comparison of the methods see the discussion just above this subsection). The solid lines show the prediction of Eq. (8) with zero-temperature values of $J_{S(D)}(\varepsilon)$ and $E_{\mathrm{ABS}}(\varepsilon)$ obtained

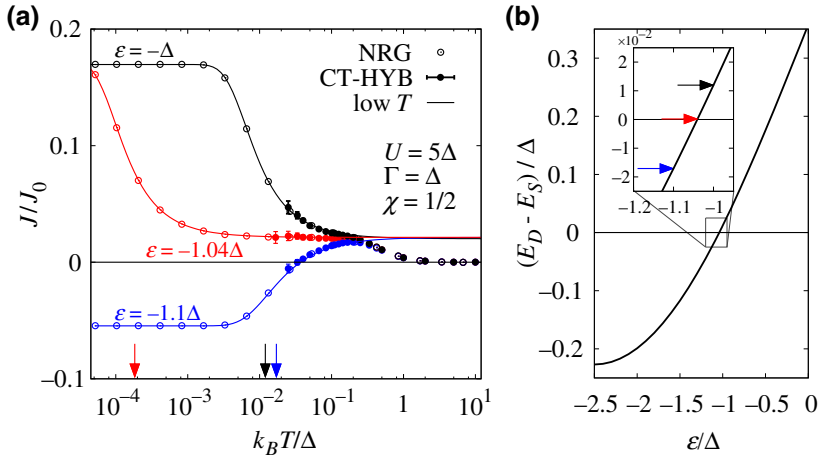

FIG. 4. (a) Low-temperature behavior of the normalized Josephson current ($J_0 \equiv 2e\Delta/\hbar$) for $U = 5\Delta$, $\Gamma = \Delta$ and $\chi = 1/2$. Empty circles with points represent NRG data, full circles with error bars are continuous-time hybridization-expansion (CT-HYB) results. The two methods agree within the QMC error bars. Solid lines correspond to the low-temperature prediction of Eq. (8) in the main text. The three lines correspond to different values of the energy level ε close to the phase boundary, so that the black line ($\varepsilon = -\Delta$) shows low-temperature behavior of the system in the 0 phase, the blue line ($\varepsilon = -1.1\Delta$) in the π phase, and the red one ($\varepsilon = -1.04\Delta$) is just slightly above the critical value. Arrows mark corresponding absolute values of zero-temperature Andreev-bound-state energies. (b) Difference between the singlet (E_S) and doublet (E_D) ground-state energy, which corresponds to the energy of the Andreev bound state. The quantum phase transition takes place at $E_D = E_S$. Inset: detail around $E_D = E_S$. Arrows mark energies corresponding to those in (a).

by the NRG. They belong to ε above, below, and very close to the critical value as shown in the inset in (b), where the zero-temperature normalized energies of the Andreev bound states $E_{\mathrm{ABS}}(\varepsilon)/\Delta$ are marked by arrows of the corresponding color. We see that the lines start as near constants in temperature at the value $J_{S(D)}(\varepsilon)$ for $k_BT \lesssim E_{\mathrm{ABS}}(\varepsilon)$ and approach $[J_S(\varepsilon) + 2J_D(\varepsilon)]/3$ for $k_BT \gtrsim E_{\mathrm{ABS}}(\varepsilon)$ with the cross-over happening at $k_BT \approx E_{\mathrm{ABS}}(\varepsilon)$ (arrows on the horizontal axis). In all cases, Eq. (8) captures perfectly the low-temperature behavior up to $k_BT \approx 0.2\Delta$. For even higher temperatures, the continuum of excitations above the gap Δ comes into play and the two-level approximation (8) necessarily breaks down.

Exactly at the QCP the singlet and doublet many-body states cross, meaning $E_S(y_C) = E_D(y_C)$. Consequently, from Eq. (8) we get the simple relation

$$X(y_C, T) = \frac{X_S(y_C) + 2X_D(y_C)}{3}, \tag{9}$$

which does not depend on temperature (within the low-temperature regime $k_BT \lesssim 0.2\Delta$ justifying the two-level approximation). We show a precise test of formula (9) with data obtained by the finite-temperature NRG in Fig. 5. The supercurrent (left panel) and average dot occupation (right panel) are plotted as functions of ε for five values of temperature. The enlargements in the vicinity of the phase-transition point prove that, indeed, at this point all lines cross and have the value determined by Eq. (9) (denoted by the horizontal dashed line). Although numerical evidence that the crossing of finite-temperature current-phase relations coincides with the QCP has been presented before (cf. Refs. [[40], Fig. 10] and [[55], Fig. 1]), as far as we are aware the relevant underlying physical mechanism expressed by Eq. (9) has not been explicitly discussed yet.

B. Determining the QCP from finite-temperature data

As Sec. IV A shows [Eq. (9) and Fig. 5], the crossing of different temperature current-phase relations may be a convenient way to straightforwardly determine the position of the QCP from finite-temperature data. However, the assumption $k_BT \ll \Delta$ used in our derivation may seem limiting and, therefore, we test this method for parameters that reflect a real experimental setup from Ref. [24]. Namely, in Fig. 6 we recalculate the example presented in the Supplemental Material of Ref. [24] with parameters reading $\Delta = 0.17$ meV, $U = 19\Delta$, $\Gamma_L + \Gamma_R = 2.6\Delta$, $a = \Gamma_L/\Gamma_R = 4$, $\varepsilon = -4.8\Delta$, and the temperature of the experiment $T_{\mathrm{exp}} = 0.076\Delta/k_B$ (150 mK). The upper panel of Fig. 6 reveals that the crossing works up to at least $T = 0.21\Delta/k_B$ (420 mK) analogously to the findings of the previous subsection. This should leave enough room for measuring a second dataset at a sufficiently higher temperature to yield another well-distinguished CPR curve, so that the position of the QCP could be read off directly from the intersection of the experimental data without any need for postprocessing.

Apart from being an unnecessary computational burden, the postprocessing itself might introduce an extra

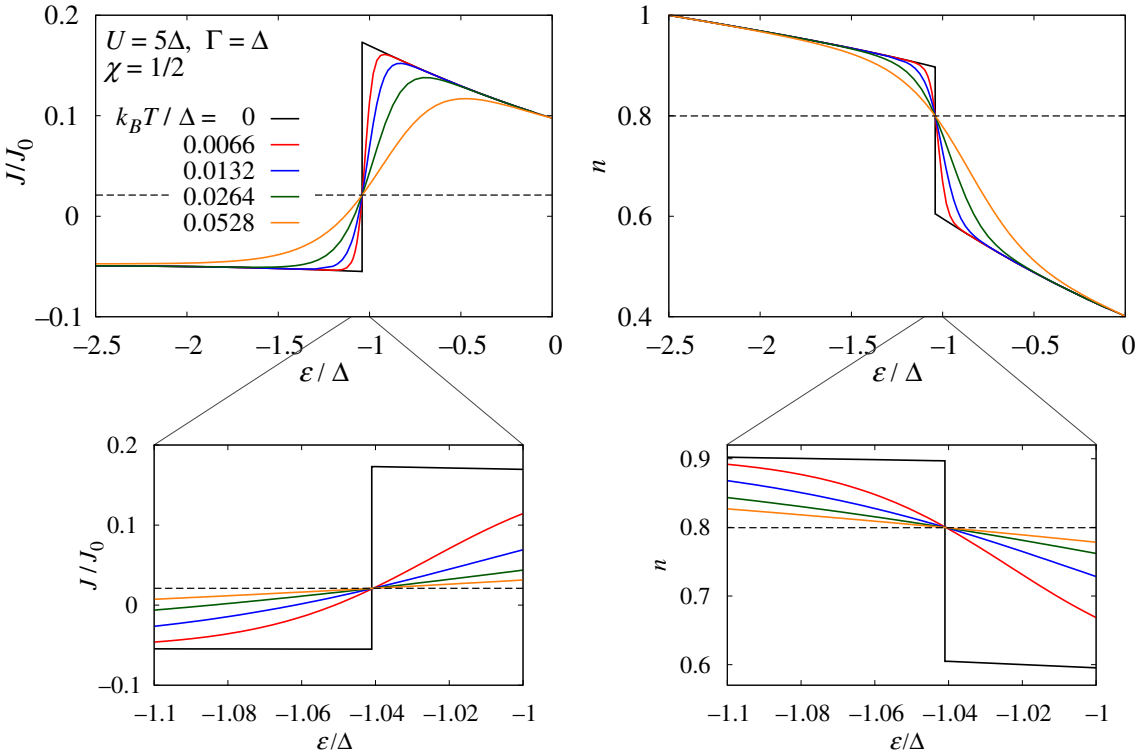

FIG. 5. The normalized supercurrent (left panel, $J_0 \equiv 2e\Delta/\hbar$) and the average dot occupation (right panel) as functions of the energy level ε for $U = 5\Delta$, $\Gamma = \Delta$, $\chi = 1/2$, and five values of temperature (in units of Δ). Horizontal dashed lines mark the values at the critical point predicted by Eq. (9), $J = [J_S + 2J_D]/3$ and $n = [n_S + 2n_D]/3$, respectively. Bottom panels are enlargements in the vicinity of the crossing points. The curves are splines of the NRG data.

error into the interpretation of the experimental data as we now demonstrate on the method used in Ref. [24] to determine the QCP. In the supplemental material the authors describe the procedure used for extracting the critical phase difference φ_C from the finite-temperature QMC data. Their numerical calculations are performed using the continuous-time interaction-expansion algorithm [53]. Few data points for each CPR $J(\varphi, T)$ for various temperatures between 145 to 580 mK are calculated and approximated by a three-term Fourier series $I(\varphi) = a_1 \sin(\varphi) + a_2 \sin(2\varphi) + a_3 \sin(3\varphi)$. The critical phase difference φ_C is then extrapolated from the zeroes $\varphi_0(T)$ of these Fourier fits for various finite temperatures using quadratic extrapolation [i.e., parabolic fit $\varphi_C - \varphi_0(T) \propto T^2$] down to $T = 0$. As the result lies very close to the zero of the measured CPR for the lowest experimental temperature 150 mK, this value is taken as the correct zero-temperature limit and thus the true critical phase.

However, our findings contradict such a conclusion. We recalculate the CPRs using the CT-HYB algorithm with more attention given to the vicinity of the zero-crossing points $J(\varphi, T) = 0$ and perform the same quadratic extrapolation, obtaining very similar results [56] shown by the black line in the bottom panel of Fig. 6. Although this procedure seems perfectly plausible, we see that φ_C obtained this way disagrees with the zero-temperature NRG result, which nevertheless coincides with the aforementioned crossing of the current-phase relations as it should.

To understand why the extrapolation method described in Supplemental Material of Ref. [24] failed to predict the correct position of the QCP, we perform the low-temperature expansion of the supercurrent using the two-level approximation (8). Using the condition $J[\varphi_0(T), T] = 0$, from Eq. (8) for the intersection point we get φ_0: $J_S(\varphi_0) + 2J_D(\varphi_0)e^{-\beta[E_D(\varphi_0) - E_S(\varphi_0)]} = 0$. We assume that the temperature is low enough so that $\varphi_0(T)$ is in the close vicinity of φ_C and can be replaced by it in the supercurrents $J_{S(D)}(\varphi_0) \simeq J_{S(D)}(\varphi_C)$. Moreover, we perform a well-justified linear expansion of the ABS energy in the exponent (see the blue curve in the inset of Fig. 6) remembering that $E_S(\varphi_C) = E_D(\varphi_C)$ at the critical point and $J(\varphi) \equiv (2e/\hbar)[dE(\varphi)/d\varphi]$ arriving at $E_D(\varphi_0) - E_S(\varphi_0) \simeq (\hbar/2e)[J_D(\varphi_C) - J_S(\varphi_C)]\,(\varphi_0 - \varphi_C)$. With these approximations we get a condition for the $\varphi_0(T)$ which reads

$$\varphi_0(T) \simeq \varphi_C + k_B T \frac{2e}{\hbar} \frac{\ln[2|J_D(\varphi_C)|] - \ln J_S(\varphi_C)}{J_D(\varphi_C) - J_S(\varphi_C)} \qquad (10)$$

and, most importantly, is *linear* in T.

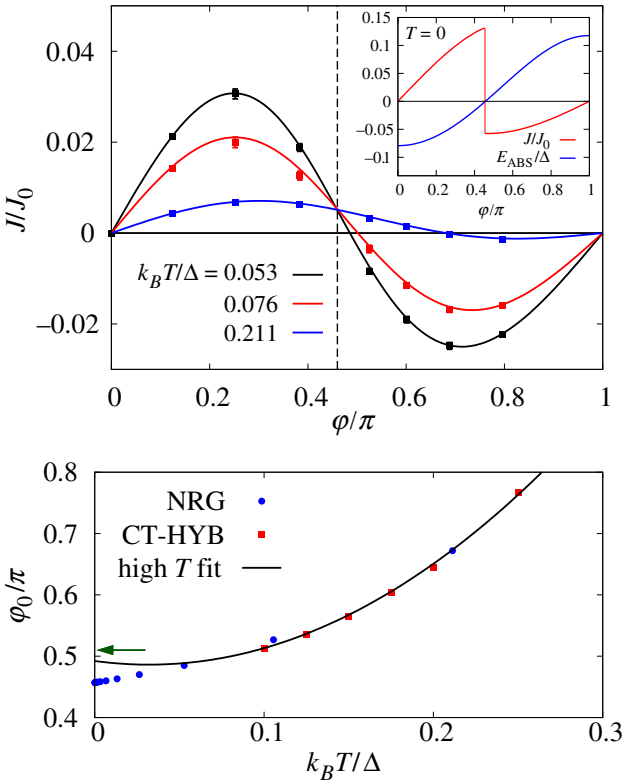

FIG. 6. Top: current-phase relations ($J_0 \equiv 2e\Delta/\hbar$) for experimental parameters taken from the Supplemental Material of Ref. [24]. Points with error bars are obtained using CT-HYB, solid lines represent the NRG results. The dashed line marks the jump in the zero-temperature NRG result for the supercurrent (see inset). The CPRs for different temperatures intersect at one point. Inset: zero-temperature supercurrent and energy of the Andreev bound state. Bottom: temperature dependence of the zero of the current-phase relation, $\varphi_0(T)$, determined by the condition $J[\varphi_0(T), T] = 0$. Blue circles represent NRG results, red squares CT-HYB data. The black solid line is a quadratic fit of the high-temperature CT-HYB data in analogy with the method used in Ref. [24]. The green arrow denotes the result of Ref. [24]. The discrepancy between the two calculations is caused by slightly different extrapolation procedures as explained in the main text.

The above replacement of φ_0 by φ_C in the supercurrents is a rather crude approximation as one can see from the inset in the upper panel of Fig. 6 where the shape of the zero-temperature CPR near φ_C is pretty steep. This limits the validity of the linear result Eq. (10) to very low temperatures only, which are typically hard to reach by the QMC (see the lower panel of Fig. 6) whose results lie already in the nonlinear regime (in Ref. [24] identified as quadratic). Extrapolation from that region (e.g., the parabolic fit in Ref. [24]) does not respect the true linear low-temperature asymptotics and, therefore, gives an erroneous estimate as can be seen in the lower panel of Fig. 6. Instead of such highly problematic and demanding extrapolation procedures (both nonlinear and linear) we strongly suggest the above crossing of finite-temperature curves as a simple, robust, and reliable method for determining the position of the quantum critical point from the finite-temperature data. It is, moreover, not limited to the phase dependence of the supercurrent only, but could be equally used for other measurable quantities as functions of any experimental control parameter.

V. CONCLUSIONS

Although currently still in their infancy and predominantly subjects of basic physical research, nanoscopic hybrid devices composed of quantum dots connected to superconducting electrodes are likely to play an important role as functional elements in future electronics technologies. One of the necessary prerequisites for achieving the transfer from fundamental physical understanding to technological applications is the development of efficient and reliable description tools for characterization and simulation of real devices. In particular, in view of today's state of the art of the theoretical description of such systems via heavy (expensive and slow) numerical techniques such as NRG or QMC, the efficiency is a critical issue.

Our work makes a step in this direction by offering simple and practical concepts and formulas for the characterization of nanoscopic superconducting hybrids generically described by the superconducting single-impurity Anderson model. We address several topics concerning the $0-\pi$ transition both in the ground state and at finite temperatures.

We present two simple analytical formulae (5) (for the weakly correlated regime) and (7) (for the Kondo regime), which capture the position of the quantum phase transition well for a wide range of parameters, especially including away from half filling. In the cross-over region, where the singlet ground state is neither purely BCS nor purely Kondo, the equations still provide at least an estimate for the critical gap (Fig. 1). Despite their approximate nature these formulas yield correct parametric dependences of the phase boundary, which is very useful for efficient scans of the parameter space needed, especially in the initial phase of the data interpretation.

For low-enough finite temperatures, which are nevertheless currently experimentally accessible (below 400 mK), the physics of the system is governed by the two lowest many-body energy levels, whose energy difference determines the energy of Andreev bound states. As a consequence the current-phase relations for different (low-enough) temperatures cross at a single point, and this crossing marks the quantum critical point (it should be stressed that this crossing point is *not* equal to the position where the supercurrent goes through zero). We propose using this crossing as an easy way how to find the quantum phase transition directly from finite-temperature data. Moreover, the crossing method is quite universal in that

it is not limited to the current-phase relation but works equally for any other quantity as a function of an arbitrary control parameter inducing the $0-\pi$ transition (Fig. 5).

Eventually, we test the status of the two state-of-the-art numerical methods (NRG and QMC) in the context of the experimentally relevant range of parameters of the superconducting single-impurity Anderson model. By extensive numerical comparisons we confirm the agreement between the NRG and QMC methods and, consequently, their reliability for modeling such Josephson junctions in the achievable range of temperatures. Even in their present implementations, they can be safely employed to pinpoint the parameter values characterizing a given device (optimally after the initial guess is framed by our analytical formulas) and for further simulations of their performance.

ACKNOWLEDGMENTS

This work is supported by the Czech Science Foundation via Project No. 16-19640S (T.N., M.Ž., A.K.), the PRIMUS/Sci/09 program of the Charles University (V.P., A.K.), the Charles University project GA UK No. 888217 (A.K.), National Science Centre (NCN, Poland) via Grant No. UMO-2017/27/B/ST3/01911 (T.N.), and the COST Action NANOCOHYBRI (CA16218) (T.N.). Computational resources are provided by The Ministry of Education, Youth and Sports from the Large Infrastructures for Research, Experimental Development and Innovations project "IT4Innovations National Supercomputing Center – LM2015070." Also, access to computing and storage facilities owned by parties and projects contributing to the National Grid Infrastructure MetaCentrum provided under the programme "Projects of Large Research, Development, and Innovations Infrastructures" (CESNET LM2015042) is greatly appreciated.

APPENDIX: MODIFIED GAL

In Refs. [46] and [47] we obtained an analytical formula for the $0-\pi$ phase boundary from the first-order spin-symmetric Hartree-Fock approximation, and noticed that its accuracy is significantly improved if the contribution from the band is neglected. Using the variables χ, $\tilde{\varepsilon}$, and $\mathcal{U}$ from the main text, the form is

$$\chi = \mathcal{U}^2 - \gamma^2\tilde{\varepsilon}^2, \tag{A1}$$

with the value of the coefficient $\gamma_{\mathrm{GAL}} = U/2\Gamma$. This formula is called the GAL [[47], Eq. (17)] in analogy with the atomic limit ($\Delta \to \infty$), where the band is also suppressed, and is found to be a surprisingly good fit to the NRG data near half filling ($\varepsilon \approx -U/2$, i.e., $\tilde{\varepsilon} \approx 0$), even competing with numerical results of the second-order diagrammatic approach.

To find a more accurate coefficient γ and thus improve the agreement away from half filling $\tilde{\varepsilon} \neq 0$, we plot the numerical data in an $\tilde{\varepsilon}^2 - \mathcal{U}$ graph and find that for $\chi = 1$ ($\varphi = 0$) the dependence is described by $1 - \tilde{\varepsilon}^2 = 1/\mathcal{U}$ for not too large Γ/Δ. Putting this condition into the dependence Eq. (A1) with γ being now a free parameter, we arrive at the value $\gamma^2 = \mathcal{U}(\mathcal{U}+1)$, which leads to the modified GAL Eq. (5).

[1] A. Martín-Rodero and A. Levy Yeyati, Josephson and Andreev transport through quantum dots, Adv. Phys. **60**, 899 (2011).

[2] S. De Franceschi, L. Kouwenhoven, C. Schönenberger, and W. Wernsdorfer, Hybrid superconductor-quantum dot devices, Nat. Nanotechnol. **5**, 703 (2010).

[3] A. F. Morpurgo, J. Kong, C. M. Marcus, and H. Dai, Gate-controlled superconducting proximity effect in carbon nanotubes, Science **286**, 263 (1999).

[4] A. Y. Kasumov, R. Deblock, M. Kociak, B. Reulet, H. Bouchiat, I. I. Khodos, Y. B. Gorbatov, V. T. Volkov, C. Journet, and M. Burghard, Supercurrents through single-walled carbon nanotubes, Science **284**, 1508 (1999).

[5] A. Kasumov, M. Kociak, M. Ferrier, R. Deblock, S. Guéron, B. Reulet, I. Khodos, O. Stéphan, and H. Bouchiat, Quantum transport through carbon nanotubes: Proximity-induced and intrinsic superconductivity, Phys. Rev. B **68**, 214521 (2003).

[6] P. Jarillo-Herrero, J. A. van Dam, and L. P. Kouwenhoven, Quantum supercurrent transistors in carbon nanotubes, Nature **439**, 953 (2006).

[7] J. A. van Dam, Y. V. Nazarov, E. P. A. M. Bakkers, S. De Franceschi, and L. P. Kouwenhoven, Supercurrent reversal in quantum dots, Nature **442**, 667 (2006).

[8] H. I. Jørgensen, K. Grove-Rasmussen, T. Novotný, K. Flensberg, and P. E. Lindelof, Electron Transport in Single-Wall Carbon Nanotube Weak Links in the Fabry-Perot Regime, Phys. Rev. Lett. **96**, 207003 (2006).

[9] J. P. Cleuziou, W. Wernsdorfer, V. Bouchiat, T. Ondarcuhu, and M. Monthioux, Carbon nanotube superconducting quantum interference device, Nat. Nanotechnol. **1**, 53 (2006).

[10] H. I. Jørgensen, T. Novotný, K. Grove-Rasmussen, K. Flensberg, and P. E. Lindelof, Critical current $0-\pi$ transition in designed Josephson quantum dot junctions, Nano Lett. **7**, 2441 (2007).

[11] K. Grove-Rasmussen, H. I. Jørgensen, and P. E. Lindelof, Kondo resonance enhanced supercurrent in single wall carbon nanotube Josephson junctions, New J. Phys. **9**, 124 (2007).

[12] E. Pallecchi, M. Gaass, D. A. Ryndyk, and C. Strunk, Carbon nanotube Josephson junctions with Nb contacts, Appl. Phys. Lett. **93**, 072501 (2008).

[13] Y. Zhang, G. Liu, and C. Lau, Phase diffusion in single-walled carbon nanotube Josephson transistors, Nano Res. **1**, 145 (2008).

[14] H. I. Jørgensen, K. Grove-Rasmussen, K. Flensberg, and P. E. Lindelof, Critical and excess current through an open quantum dot: Temperature and magnetic-field dependence, Phys. Rev. B **79**, 155441 (2009).

[15] G. Liu, Y. Zhang, and C. N. Lau, Gate-Tunable Dissipation and "Superconductor-Insulator" Transition in Carbon Nanotube Josephson Junctions, Phys. Rev. Lett. **102**, 016803 (2009).

[16] A. Eichler, R. Deblock, M. Weiss, C. Karrasch, V. Meden, C. Schönenberger, and H. Bouchiat, Tuning the Josephson current in carbon nanotubes with the Kondo effect, Phys. Rev. B **79**, 161407 (2009).

[17] C. B. Winkelmann, N. Roch, W. Wernsdorfer, V. Bouchiat, and F. Balestro, Superconductivity in a single-C_{60} transistor, Nat. Phys. **5**, 876 (2009).

[18] J.-D. Pillet, C. H. L. Quay, P. Morfin, C. Bena, A. L. Yeyati, and P. Joyez, Andreev bound states in supercurrent-carrying carbon nanotubes revealed, Nat. Phys. **6**, 965 (2010).

[19] G. Katsaros, P. Spathis, M. Stoffel, F. Fournel, M. Mongillo, V. Bouchiat, F. Lefloch, A. Rastelli, O. Schmidt, and S. De Franceschi, Hybrid superconductor–semiconductor devices made from self-assembled SiGe nanocrystals on silicon, Nat. Nanotechnol. **5**, 458 (2010).

[20] R. Maurand, T. Meng, E. Bonet, S. Florens, L. Marty, and W. Wernsdorfer, First Order $0-\pi$ Quantum Phase Transition in the Kondo Regime of a Superconducting Carbon Nanotube Quantum Dot, Phys. Rev. X **2**, 011009 (2012).

[21] E. J. H. Lee, X. Jiang, R. Aguado, G. Katsaros, C. M. Lieber, and S. De Franceschi, Zero-Bias Anomaly in a Nanowire Quantum Dot Coupled to Superconductors, Phys. Rev. Lett. **109**, 186802 (2012).

[22] J. D. Pillet, P. Joyez, R. Žitko, and M. F. Goffman, Tunneling spectroscopy of a single quantum dot coupled to a superconductor: From Kondo ridge to Andreev bound states, Phys. Rev. B **88**, 045101 (2013).

[23] A. Kumar, M. Gaim, D. Steininger, A. L. Yeyati, A. Martín-Rodero, A. K. Hüttel, and C. Strunk, Temperature dependence of Andreev spectra in a superconducting carbon nanotube quantum dot, Phys. Rev. B **89**, 075428 (2014).

[24] R. Delagrange, D. J. Luitz, R. Weil, A. Kasumov, V. Meden, H. Bouchiat, and R. Deblock, Manipulating the magnetic state of a carbon nanotube Josephson junction using the superconducting phase, Phys. Rev. B **91**, 241401(R) (2015).

[25] R. Delagrange, R. Weil, A. Kasumov, M. Ferrier, H. Bouchiat, and R. Deblock, $0-\pi$ quantum transition in a carbon nanotube Josephson junction: Universal phase dependence and orbital degeneracy, Phys. Rev. B **93**, 195437 (2016).

[26] S. Li, N. Kang, P. Caroff, and H. Q. Xu, $0-\pi$ phase transition in hybrid superconductor-InSb nanowire quantum dot devices, Phys. Rev. B **95**, 014515 (2017).

[27] R. Delagrange, R. Weil, A. Kasumov, M. Ferrier, H. Bouchiat, and R. Deblock, $0-\pi$ quantum transition in a carbon nanotube Josephson junction: Universal phase dependence and orbital degeneracy, Phys. B **536**, 211 (2018).

[28] L. Farinacci, G. Ahmadi, G. Reecht, M. Ruby, N. Bogdanoff, O. Peters, B. W. Heinrich, F. von Oppen, and K. J. Franke, Tuning the Coupling of an Individual Magnetic Impurity to a Superconductor: Quantum Phase Transition and Transport, Phys. Rev. Lett. **121**, 196803 (2018).

[29] V. Bouchiat, Detection of magnetic moments using a nano-squid: Limits of resolution and sensitivity in near-field squid magnetometry, Supercond. Sci. Technol. **22**, 064002 (2009).

[30] D. J. Luitz, F. F. Assaad, T. Novotný, C. Karrasch, and V. Meden, Understanding the Josephson Current Through a Kondo-Correlated Quantum Dot, Phys. Rev. Lett. **108**, 227001 (2012).

[31] W. Chang, V. E. Manucharyan, T. S. Jespersen, J. Nygård, and C. M. Marcus, Tunneling Spectroscopy of Quasiparticle Bound States in a Spinful Josephson Junction, Phys. Rev. Lett. **110**, 217005 (2013).

[32] T. Matsuura, The effects of impurities on superconductors with Kondo effect, Prog. Theor. Phys. **57**, 1823 (1977).

[33] L. I. Glazman and K. A. Matveev, Resonant Josephson current through Kondo impurities in a tunnel barrier, JETP Lett. **49**, 659 (1989).

[34] A. V. Rozhkov and D. P. Arovas, Josephson Coupling Through a Magnetic Impurity, Phys. Rev. Lett. **82**, 2788 (1999).

[35] T. Yoshioka and Y. Ohashi, Numerical renormalization group studies on single impurity Anderson model in superconductivity: A unified treatment of magnetic, nonmagnetic impurities, and resonance scattering, J. Phys. Soc. Jpn. **69**, 1812 (2000).

[36] F. Siano and R. Egger, Josephson Current Through a Nanoscale Magnetic Quantum Dot, Phys. Rev. Lett. **93**, 047002 (2004).

[37] M.-S. Choi, M. Lee, K. Kang, and W. Belzig, Kondo effect and Josephson current through a quantum dot between two superconductors, Phys. Rev. B **70**, 020502 (2004).

[38] G. Sellier, T. Kopp, J. Kroha, and Y. S. Barash, π junction behavior and Andreev bound states in Kondo quantum dots with superconducting leads, Phys. Rev. B **72**, 174502 (2005).

[39] T. Novotný, A. Rossini, and K. Flensberg, Josephson current through a molecular transistor in a dissipative environment, Phys. Rev. B **72**, 224502 (2005).

[40] C. Karrasch, A. Oguri, and V. Meden, Josephson current through a single Anderson impurity coupled to BCS leads, Phys. Rev. B **77**, 024517 (2008).

[41] T. Meng, S. Florens, and P. Simon, Self-consistent description of Andreev bound states in Josephson quantum dot devices, Phys. Rev. B **79**, 224521 (2009).

[42] A. Camjayi, L. Arrachea, A. Aligia, and F. von Oppen, Fractional Spin and Josephson Effect in Time-Reversal-Invariant Topological Superconductors, Phys. Rev. Lett. **119**, 046801 (2017).

[43] A. Kadlecová, M. Žonda, and T. Novotný, Quantum dot attached to superconducting leads: Relation between symmetric and asymmetric coupling, Phys. Rev. B **95**, 195114 (2017).

[44] K. G. Wilson, The renormalization group: Critical phenomena and the Kondo problem, Rev. Mod. Phys. **47**, 773 (1975).

[45] F. D. M. Haldane, Theory of the atomic limit of the Anderson model. I. Perturbation expansions re-examined, J. Phys. C **11**, 5015 (1978).

[46] M. Žonda, V. Pokorný, V. Janiš, and T. Novotný, Perturbation theory of a superconducting $0-\pi$ impurity quantum phase transition, Sci. Rep. **5**, 8821 (2015).

[47] M. Žonda, V. Pokorný, V. Janiš, and T. Novotný, Perturbation theory for an Anderson quantum dot asymmetrically

attached to two superconducting leads, Phys. Rev. B **93**, 024523 (2016).
[48] V. Pokorný, SQUAD – second-order perturbation theory solver for a superconducting quantum dot (2016), github.com/pokornyv/SQUAD.
[49] R. Žitko, NRG Ljubljana – open source numerical renormalization group code (2014), nrgljubljana.ijs.si.
[50] J. Bauer, A. Oguri, and A. C. Hewson, Spectral properties of locally correlated electrons in a Bardeen–Cooper–Schrieffer superconductor, J. Phys.: Cond. Mat. **19**, 486211 (2007).
[51] Note that the Kondo temperature Eq. (3) is also an approximation valid around $\tilde{\varepsilon} \approx 0$.
[52] P. Seth, I. Krivenko, M. Ferrero, and O. Parcollet, TRIQS/CTHYB: A continuous-time quantum Monte Carlo hybridisation expansion solver for quantum impurity problems, Comput. Phys. Commun. **200**, 274 (2016).
[53] D. J. Luitz and F. F. Assaad, Weak-coupling continuous-time quantum Monte Carlo study of the single impurity and periodic Anderson models with s-wave superconducting baths, Phys. Rev. B **81**, 024509 (2010).
[54] V. Pokorný and M. Žonda, Correlation effects in superconducting quantum dot systems, Phys. B **536**, 488 (2018).
[55] M.-S. Choi, M. Lee, K. Kang, and W. Belzig, Comment on "Josephson Current Through a Nanoscale Magnetic Quantum dot", Phys. Rev. Lett. **94**, 229701 (2005).
[56] The reason why our zero-temperature extrapolation does not coincide precisely with the previous calculation (marked by the green arrow) is most probably the Fourier fitting, which we could avoid.